RSC Advances

ROYAL SOCIETY OF CHEMISTRY

www.rsc.org/advances

Plasmonic photocatalyst Ag@AgCl/$ZnSn(OH)_6$: Synthesis, characterization and enhanced visible-light photocatalytic activities in the decomposition of dyes and phenol

Fei Chen[a,b], Qi Yang[a,b,*], Chenggang Niu[a,b], Xiaoming Li[a,b], Chang Zhang[a,b], Guangming Zeng[a,b]

[a] College of Environmental Science and Engineering, Hunan University, Changsha 410082, P.R. China

[b] Key Laboratory of Environmental Biology and Pollution Control (Hunan University), Ministry of Education, Changsha 410082, P.R. China

Author information

First author: E-mail: feichen@hnu.edu.cn (Fei Chen)

*Corresponding author:E-mail: Yangqi@hnu.edu.cn

ABSTRACT

An efficient visible-light-driven photocatalyst Ag@AgCl/$ZnSn(OH)_6$ (Ag@AgCl/ZSH) was successfully fabricated by an ultrasonic assistant precipitation-photoreduction method at room temperature. The photophysical properties of the as-prepared samples were characterized by X-ray diffraction (XRD), Fourier transform infrared spectroscopy (FTIR), scanning electron microscopy (SEM), transmission electron microscopy (TEM), Energy disperse X-ray (EDX), UV-vis diffuse reflectance spectroscopy (DRS), X-ray photoelectron spectroscopy (XPS), and photoluminescence emission spectra (PL) analysis. The photocatalytic activities of the as-prepared samples were evaluated by the photodegradation of rhodamine B (RhB), crystal violet (CV) and phenol aqueous solution. The Ag@AgCl (8wt%)/ZSH-20 composite exhibited the optimal photocatalytic performance, and the corresponding degradation rates for RhB, CV and phenol solution were as higher as 22/3.6, 15/4 and 16/3.6 times to those of pure ZSH and the conventional visible-light photocatalyst N-TiO_2, respectively. The photo-reduction time upon the photocatalytic properties for the Ag@AgCl/ZSH composites were systematically investigated. Moreover, a possible degradation mechanism was proposed by reaction equations and simulated scheme on the basis of active species trapping experiment and band energy analysis. The dramatically enhanced photocatalytic performance of Ag@AgCl/ZSH should be ascribed to the surface plasmon resonance (SPR) effect from Ag@AgCl nanoparticles and high separation of photogenerated electron-hole pairs in the photocatalytic process, leading to the low recombination rates of the photoinduced

electron-hole pairs. High degradation efficiencies and physicochemical features were maintained after five recycling experiments, indicating that the photocatalysts were relatively durable and stable. It is expected that the plasmonic photocatalyst Ag@AgCl/ZSH is a promising candidate material for the photodegradation of organic pollutants in wastewater.

Keywords: Visible-light-driven; Ag@AgCl/ZSH; Degradation; Photocatalytic; Surface plasmon resonance.

1. Introduction

Over the past decades, semiconductor photocatalysis, as a novel and renewable technology, has aroused considerably scientific and industrial awareness due to its potential in solving environment pollution and energy crisis issues which seriously threaten our survival. [1-5] To date, TiO_2 has been deemed to be the most extensively employed semiconductor material for a long time and proved to be effective in the decomposition of harmful organic substrates and hydrogen production, owing to its excellent photocatalytic properties, superior chemical stability, non-toxic nature, and low-cost. [6-8] Nevertheless, the practical application of TiO_2 (3.0-3.2 eV) photocatalyst in industrial production was restricted by the high recombination of photo-generated electron-hole pairs within photocatalytic materials and relatively low efficiency use of solar energy.[9, 10] Hence, it is urgent to explore a new efficient photocatalyst, which could satisfy the requirement of industrial production applications.

So far, many kinds of new-type semiconductor photocatalysts have been designed and investigated such as In_2O_3,[11] $Bi_2O_2CO_3$,[12] Cu_2O,[13] BiOBr,[14] InOOH,[15] ZSH[16] and so on, because of their potential applicability in the degradation of harmful organic contaminants. Considering of the non-toxicity and safety properties, ZSH has been widely utilized in highly effective flame retardants, smoke inhibitor, inorganic filler, gas-sensing material and photodegradation of organic pollutants.[16-19] As a kind of perovskite-structured hydroxide, the surface of ZSH is full of OH groups which can accept photogenerated holes to form hydroxyl radicals (OH), and the forming OH played a vital role in photocatalytic reactions.[20] In recent years, ZSH had been applied successively in the photodegradation of organic pollutions. For example, Fu et al. had successfully fabricated the cube-shaped ZSH by a solvethermal process, and the as-prepared photocatalyst exhibited excellent photocatalytic performance to degrade

benzene under UV irradiation.[21] Chen et al. prepared ZSH nanoparticles by homogeneous precipitation (HP) and hydrothermal (HT) method, which showed much superior photocatalytic activities in the degradation of methyl orange and benzene compared with pure TiO_2 under UV irradiation.[16] In addition, for accelerating the separation of charge carriers and reducing the recombination of electron-hole pairs, Li and his co-workers had successfully established the heterojunction structure between ZSH and BiOI, which expanded the optical response to the visible region and the absorption edge shifted to longer wavelengths.[22] Superficially, the aforementioned modified ZSH have achieved efficient photocatalytic activities to some extent, but most of improved photocatalytic performance is restricted in UV light region. In order to make better use of the inexpensive, earth-abundant solar energy, it is imperative to develop more efficient modified method to solve the drawbacks of single-component photocatalyst ZSH and improve the separation of photo-generated electron-hole pairs in the photocatalysis process.

Up to now, a large number of visible-light-driven (VLD) photocatalysts have been developed combining with the strategy of surface plasmon resonance (SPR), which can be realized through the collect oscillation of free electrons on the surface of noble-metal nanoparticles (such as Au, Ag and Pt). It is generally recognized that noble metal nanoparticles (NPs) had broadened the absorption in the visible-light region attributing to the SPR structure, further to improve the photocatalytic performance in degradation of organic pollutants. [23, 24] In particular, the silver/silver halides (denoted as Ag/AgX, X = Cl, Br, I) have gained considerable attention in both scientific and engineering field and have been considered as an alternative attractive visible-light-driven photocatalyts, as a consequence of their outstanding photocatalytic performances in the decomposition of organic pollutants, [25, 26] water

splitting, [27] carbon dioxide reduction [28] under visible-light irradiation. Inspired by the photosensitive properties and the SPR effect of Ag NPs, a wide range of attention and concern has concentrated in the developing of high efficient plasmonic Ag/AgX photocatalysts [29, 30]. More importantly, Ag/AgX-based composite photocatalysts had been decorated successfully in recent years with efficient interfacial charge transfer and high photo-induced charge separation [31, 32], such as Ag/AgCl/TiO_2 [33], Ag/AgI/Al_2O_3.[25] Ag/AgCl/WO_3, [34] Ag/AgCl/g-C_3N_4, [35] Ag/AgCl/Bi_2WO_6, [36] AgI/TiO_2. [37] These new composite photocatalysts were verified to excellent VLD (visible-light-driven) photocatalysts, they could expand the spectral range of light absorption and significantly enhanced the energy utilization efficiency. It can be deduced from the above conclusions that Ag/AgX is not only as an active photocatalyst, but also a potential co-catalyst. The combination of ZSH with Ag/AgCl nanoparticles could elevate the efficiency of electron-hole separation and further to achieve the highly efficient utilization of solar energy. However, to date, still very few works have been reported on synthesis and application of this new-type composite.

In the present work, a facile ultrasonic assistant precipitation-photoreduction reaction approach was used to prepare Ag/Ag/ZSH composite, a visible-light photocatalyst. The photocatalytic activities of the as-prepared samples were systematically evaluated by decomposition of organic dyes and phenol under visible light irradiation. Moreover, the possible photocatalytic mechanism for the enhanced photocatalytic performance was elaborated in detail. This work may provide a platform to design novel VLD photocatalysts for practical application.

2. Experimental

2.1 Materials

Zinc acetate dehydrate ($Zn(CH_3COO)_2 \cdot 2H_2O$, tin chloride pentahydrate ($SnCl_4 \cdot 5H_2O$), sodium hydroxide (NaOH), Polyvinyl pyrrolidone (PVP), Silver nitrate ($AgNO_3$), Cetanecyl Trimethyl Ammonium Chloride (CTAC) and ethanol were purchased from Sinopharm Chemical Reagent Co., Ltd. Rhodamine B (RhB, simple dye), crystal violet (CV, solid dye, Changsha Dyeing and Printing Factory) and phenol were chosen as the target substances to evaluate the photocatalytic properties of the as-prepared samples. All chemicals were analytical reagent grade and used without additional purification or treatment. Deionized water was used as the solvent throughout the experiment.

2.1 Synthesis of ZSH nanocubes

ZSH nanocubes were fabricated by a chemical bath approach under mild conditions. A typical systhesis procedure was as follows: Firstly, 5 mmol Zn-$(CH_3COO)_2 \cdot 2H_2O$ and 0.5 g PVP were dissolved in 25 ml of deionized water with magnetic stirring. Secondly, 25 ml of $SnCl_4 \cdot 5H_2O$ (0.2 M) was added dropwise into the above $Zn(CH_3COO)_2 \cdot 2H_2O$ solution. With constant stirring, 100 ml of NaOH solution (0.6 M) was added slowly into the solution. After being continuous stirring for 30 min at room temperature, the mixed solution was aged at 60 °C for 6 h. When the mixture was cooled down to room temperature naturally, the resulting white precipitate was collected by filtering and washing with deionized water and ethanol for several times to remove the ions and surfactant possibly remaining in the forming products. At last, the products were dried at 80 °C in air for 8 h.

2.2 Sythesis of Ag/AgCl/ZSH

The preparation of Ag/AgCl/ZSH composites was achieved by an ultrasonic assistant precipitation-photoreduction reaction. Briefly, 0.5 g ZSH nanocube and 0.4 g of CTAC was added into 40 ml deionized water. The introduction of CTAC not only played a role of surfactant but also served as the source of Cl^- in the as-prepared samples. The excessive CTAC resulted in homogeneously dispersed AgCl and induced Cl^- to precipitate Ag^+ in the suspension. After being ultrasonicated for 20 min, the suspension was magnetically stirred for 1 h at room temperature. Then, a certain amount of $AgNO_3$ (0.1 M) solution was dripped added into the above solution. The forming mixture was ultrasonicated for 20 min and afterwards stirred under a dark condition for another 1 h. Subsequently, the resulting suspension was placed under irradiation of a 40 W ultraviolet lamp for the indicted lengths of time. In the exposure duration under UV light irradiation, the color of the as-prepared sample changed from white to grayish, and the resultant grayish product was finally collected by centrifugation, washed with ethanol and deionzied water thoroughly and dried at 80 °C for 8 h. According to the weight ratio of Ag to ZSH, the obtained products were noted as Ag@AgCl (2 wt%)/ZSH, Ag@AgCl (4 wt%)/ZSH, Ag@AgCl (8 wt%)/ZSH, Ag@AgCl (14 wt%)/ZSH, respectively. Furthermore, Ag@AgCl/ZSH-10, Ag@AgCl/ZSH-20, Ag@AgCl/ZSH-30, Ag@AgCl/ZSH-40 represents the samples prepared under 10, 20, 30, and 40 min of photoreduction, respectively.

To have a better comparison, Ag-ZSH, AgCl-ZSH and Ag@AgCl were also prepared by the same procedures in the absence of CTAC, $AgNO_3$ and ZSH, respectively for the photodegradation of RhB solution. Additionally,

visible-light-active N-doped TiO_2 was also prepared by nitridation of commercial TiO_2 at 500 °C for 10 h under NH_3 flow [38] which was used as the reference to further evaluate the photocatalytic performance of the catalysts.

2.3 Characterization

The phase compositions of as-prepared samples were characterized by using X-ray diffraction (Rigaka D/max 2500v/pc X-ray with Cu Ka radiation at a scan rate of 0.1° 2θ s^{-1}. The working voltage and the applied current of the diffraction were 40 kV and 40 mA, respectively. Fourier transform infrared spectrometer (FTIR) spectra were collected on an IR Prestige-21 spectrometer (Shimadzu, Japan) at the room temperature by the standard KBr disk method. The morphologies of the samples were investigated with a field emission scanning electron microscope (FESEM, Hitachi S-4800) with 5.0 kV scanning voltages. The transmission electron microscope (TEM) was carried out with a transmission electron microscope (TEM, FEI Tecnai G20) at an accelerating voltage of 200 kV). The elementary composition of the as-prepared samples was investigated by Energy dispersive X-ray (EDX) analysis attached to the Techai G20. UV-vis diffuse reflectance spectrum (DRS) was performed at room temperature on a Shimadza UV-4100 UV-vis spectrometer in the range of 200-800 nm, using $BaSO_4$ as the reference. The chemical states of the as-prepared samples were analyzed by X-ray photoelectron spectroscopy (XPS) using a Thermo ESCALAB 250XI spectrometer with Al Kα source. The PL spectra of the photocatalysts were monitored using a transient fluorescence spectrometer (Edinburgh FLsp920 full functional state) with excitation wavelength of 208 nm.

2.4 Photocatalytic Test

The photocatalytic activities of Ag@AgCl/ZSH composites were evaluated by the decomposition of organic dyes and phenol in aqueous solution under visible-light irradiation using a 300 W Xe lamp with a cutoff filter (λ > 420 nm). In each experiment, the catalysts were added into rhodamine B (RhB, 10 mg/L, 100 mL), crystal violet (CV, 10 mg/L, 100 mL), and phenol solution (10 mg/L, 100 mL), and the corresponding amounts of the catalysts were 0.04 g, 0.1 g, 0.1 g, respectively. Prior to irradiation, the solution was constantly stirred in dark for 30 min to ensure the adsorption-desorption equilibrium of organic pollutants on the surface of the catalysts. Afterwards, the mixture was exposed to visible light irradiation with a 20 cm distance height (the distance from the cut off filter to the liquid surface). At given interval, 4 mL analytical samples were taken and then centrifuged (8000 rpm, 4 min) to remove the residual photocatalyst powder. The concentration of organic pollutants was measured by monitoring the maximum absorption peak in the ultraviolet visible spectrum (wavelength from 200 nm to 700 nm) by a UV-visible Spectrophotometer (Shimadzu 2550, Japan) with deionized water as a reference sample.

As a comparison, photocatalytic activitie of single organic pollutant in the absence of photocatalyst and N-doped TiO_2 were also tested under the same experimental conditions.

3. Result and discussion

3.1 Characterization of Ag@AgCl/ZSH composite

3.1.1 XRD analysis

The crystallographic structures of as-prepared ZSH and Ag@AgCl/ZSH samples with different photoreduction time were confirmed by XRD patterns. As shown in Figure 1, pure ZSH could be indexed as the standard cubic phase of ZSH (JCPDS file NO. 73-2384 [20]). The diffraction peaks of the samples are sharp and intense, confirming that ZSH cubic crystallites with high purities could be obtained under facile chemical bath. As clearly marked in Figure 1, intense diffraction peaks at 19.79°, 22.89°, 32.58°, 36.56°, 38.14°, 40.19°, 52.65° and 58.13°, which could be assigned to ZSH (111), (200), (220), (013), (311), (222), (420), (422), respectively. From the XRD patterns, the peaks at 27.83°, 32.24°, 46.22° could be indexed to the (111), (200), (220) crystal planes of AgCl. Another weak peak appearing at 40.19° could be attributed to (112) plane of Ag. All the characteristic peaks belonging to cubic ZSH were also discovered in the XRD patterns of Ag@AgCl/ZSH composites , indicating that the introducing of Ag@AgCl didn't destroy the phase structure of ZSH. Taken the XRD patterns of different photo-reduction time into consideration, the peaks corresponding to AgCl became weaker with the increased exposure time under UV-light irradiation, suggesting that Ag^+ ion of AgCl was converting to Ag^0 species by UV light irradiation.

3.1.2 SEM analysis

The typical SEM images of as-prepared ZSH and Ag@AgCl/ZSH-20 composite were presented in Figure 2. It could be clearly seen that the pure ZSH sample possessed uniform and cubic-like morphology with a length of 200-500 nm. For Ag@AgCl/ZSH-20 composite, a few small nanoparticles are attached to the edge and

the vicinity of the nanocubes, which could be ascribed to the Ag@AgCl NPs. Besides, the size and morphology of Ag@AgCl/ZSH-20 sample presented as the same as the pure ZSH with the addition of Ag@AgCl, consistent with the XRD results.

3.1.3 TEM and EDX analysis

The TEM images and EDX result of Ag@AgCl/ZSH-20 photocatalyst were presented in Figure 3. From Figure 3 (a, b, c), it is easy to find out that cubic-like structure, which belonged to ZSH composite. Synchronously, a few small nanoparticles of about 10-200 nm also were observed on the surface of ZSH, which could be assigned to the Ag@AgCl nanoparticles. Figure 3d displays a typical EDX spectrum obtained from the Ag@AgCl/ZSH-20 sample, it could be clearly seen that Zn, Sn, O, Ag, Cl were all coexisting. The molar ratio of Ag and Cl is about 1.2, which is higher than the theoretic stoichiometric atomic ratio between Ag and Cl species in the pure AgCl. The result confirms the existence of excessive Ag on the surface of Ag@AgCl/ZSH-20 composite.

3.1.4 XPS analysis

In order to determine quantitative information in regard to the chemical composition, surface electronic state and the nature of the functional groups involved in Ag@AgCl/ZSH composites, X-ray photoelectron spectroscopy (XPS) measurement was performed and the results are shown in Figure 4. Figure 4a is the XPS survey spectra of Ag@AgCl/ZSH-20. It can be found that the sample contains not only Zn, Sn, O, but also C, Ag and Cl elements. The emergence of C (the peak at 284.57 eV) could be assigned to the adventitious hydrocarbon from the XPS instrument itself. [33,

[36] A typical Zn 2p XPS spectrum of the sample exhibited the predominant characteristic peak at 1021.59 eV (Figure 4b). Two main peaks (Figure 4c) appeared at the binding energies of 486.6 eV and 495.0 eV belonged to the Sn $3d_{5/2}$ and Sn $3d_{3/2}$, respectively. From the Cl 2p spectra (Figure 4d), two peaks are observed at about 197.7 eV and 199.3 eV, which correspond to Cl $2p_{3/2}$ and Cl $2p_{1/2}$, respectively. Learning from Figure 4e, the Ag 3d spectra of Ag@AgCl/ZSH-20 consisted of two individual peaks belong to Ag $3d_{3/2}$ and Ag $3d_{5/2}$, of which the corresponding binding energies were 373 eV and 367 eV, respectively. These two peaks could be further divided into two peaks, at about 373.74/374.33 eV and 367.74/368.64 eV, respectively. According to the previous studies, the peaks at 373.74 and 367.74 eV are attributing to Ag^+ of AgCl, and those at 374.33 and 368.64 eV are due to Ag^0 of AgCl. [31, 34] The XPS result of Ag 3d confirmed the existence of metallic Ag in the Ag@AgCl/ZSH composite, in accord with the above-described XRD analysis. However, the appropriate amount of silver in the forming Ag@AgCl/ZSH composites is quietly important. The ratio of the Ag^0/Ag^+ increased with the increasing photo-reduction time under UV light irradiation, indicating that the excessive amount of silver might have been produced, leading to lower efficiency in the photocatalytic efficiency.

3.1.5 FTIR analysis

Fourier transform infrared spectroscopy (FTIR) was employed to analyze the chemical bonding and composition of the as-prepared samples. As shown in Figure 5, the spectrum of ZSH is quite similar to ZSH reported previously.[19] Two bands at about 3222 cm^{-1} and 1628 cm^{-1} are attributing to the O-H stretching vibration and

bend vibration, respectively. The peak observed at 1174 cm^{-1} is due to the Sn-OH bending. Another two peaks found at 776 cm^{-1} and 542 cm^{-1} could be ascribed to the water-water hydrogen banding and Sn-O stretching vibration, respectively. As for Ag@AgCl/ZSH-20 composite, the similar absorption bands could also be discovered, the difference was detected that the absorption bands showed little weakened for the Ag@AgCl deposited on the surface of the as-prepared ZSH sample. The above results indicate that the structure of ZSH was not changed with the addition of Ag@AgCl, which in good accordance with the XRD analysis.

3.1.6 UV-vis diffuse reflectance spectrum

The optical absorption properties of as-preapared samples were determined by UV-vis diffuse reflectance spectrum. As illustrated in Figure 6, the pure ZSH only presents absorption in the UV light region, with an absorption edge about 334 nm. The band gap of ZSH was estimated to 3.71 eV according to the relationship (E_g=1240/λ, [26, 39] where λ is the absorption edge and E_g is the corresponding band gap), the result was consistent with the previous reports.[20] However, Ag@AgCl/ZSH-20 exhibited broad absorption in both ultraviolet and visible region, especially between 400 nm and 800 nm is intensively increased owing to the surface plasmon resonance (SPR) adsorption of Ag nanoparticles on the surface of ZSH.[40, 41]

3.2 Photocatalytic activity measurements

The photocatalytic activities of Ag@AgCl/ZSH photocatalysts were evaluated by photodegradation of rhodamine B (RhB), crystal violet (CV) and phenol in aqueous solution under visible light irradiation, respectively. In the photodegradation processes,

RhB solution was chosen as the target pollutant to determine the optimum dosage of Ag@AgCl nanoparticles and the results are shown in Figure 7. The pure ZSH exhibited poor photocatalytic activity, resulting in less than 10 % of RhB reduction after 60 min irradiation. Because of the introduction of Ag@AgCl on the surface of the ZSH, the photocatalytic activity of ZSH had been enhanced largely and increased with the increasing weight ratio of Ag to ZSH. However the weight ratio of 14 wt% composite showed a little higher photocatalytic activity than that of 8 wt%, so Ag@AgCl (8 wt%)/ZSH was employed in the following research considering of the low-price and long-term application. For comparison, Ag-ZSH, AgCl-ZSH, Ag@AgCl, were also prepared to further confirm the excellent photocatalytic activity of Ag@AgCl/ZSH, Figure S1 showed that the as-prepared Ag@AgCl (8 wt%)/ZSH displayed the highest photodegradation efficiency of RhB solution. The time-dependent UV-vis absorption of RhB and CV dyes during the visible light irradiation were demonstrated in Figure 8. It can be seen clearly that the maximum absorbance decreased dramatically after visible light irradiation within 60 min for the as-prepared ZSH nanocubes, N-doped TiO_2 and Ag@AgCl/ZSH-20 photocatalyst. Figure 9 revealed the photodegradation of RhB and CV dyes as a function of visible light irradiation time for the various Ag@AgCl/ZSH photocatalysts. According to the above analysis, the photocatalytic activities of the as-prepared samples with different photo-reduction time increased at first 20 min and decreased with the increase of photo-reduction time up to 40 min. Besides, pure ZSH and N-doped TiO_2 were also tested under the same experimental condition to assess the highly enhanced

photocatalytic activities of the as-synthesized Ag@AgCl/ZSH composites. The obtained results proved that Ag@AgCl/ZSH photocatalysts exhibited highly improved photocatalytic activities in both degradation of RhB and CV solution, of which Ag@AgCl/ZSH-20 presented the most pronounced photocatalytic properties. The degradation efficiencies of RhB and CV could reach to 99.86% and 98.56 % in the irradiation time of 60 min, while the pure ZSH could only decompose a small amount of the dyes solution. The photocatalytic activity of N-TiO_2 was examined under the same operational condition; only 67.12% of RhB and 33.66 % of CV solution were decomposed within 60 min. Further to determine the excellent photocatalytic activity of Ag@AgCl/ZSH-20 composite, phenol (representative of refractory organics) was chosen as the objective. As precisely shown in Figure 10, the superior photodegradation efficiency of phenol was about 91% with the irradiation time of 120 min. The enormous potentiality of photodegrdation of complex organic pollutants was manifested in view of the aforementioned analysis.

The photocatalytic degradation of organic pollutants on different catalysts was investigated by the pseudo first-order kinetic and clearly shown in Figure 11. The rate constants could be calculated by the following equation: [42]

$$\ln (C_0/C_t) = - k_{app}\, t \qquad (1)$$

where C_t is the concentration of pollutants at the time of t (mg/l), C_0 is the initial concentration of the pollutants (mg/l) and k_{app} is the apparent pseudo first-order rate constant). All of the reactions had a good linearity, indicating that visible-light-driven photodegradation of RhB and CV solutions in the presence of the photocatalysts

followed the first order kinetics.

The corresponding degradation rates (k) and relative coefficient (R^2) of decomposition of RhB and CV aqueous solution were labeled obviously in Figure S2. Higher R^2 values (>0.98) indicated that visible-light-driven photodegradation of RhB and CV solutions in the presence of the photocatalysts followed the pseudo first-order kinetics. It could be concluded that Ag@AgCl/ZSH-20 sample presented as the highest degradation rate in the photodegradation of RhB and CV, respectively. When taking the pure ZSH and N-doped TiO_2 into comparison, the corresponding of degradation rate constant of Ag@AgCl/ZSH-20 is estimated to be 0.06652 min^{-1} in the decomposition of RhB solution, which is up to 22-fold faster than that over bare ZSH and up to 3.6-fold faster than that over N-TiO_2. Simultaneously, for CV photodegradation, it was 15 and 4 times higher than that of pure ZSH and N-doped TiO_2 by Ag@AgCl/ZSH-20 sample. What's more, the direct non-catalyst photocatalysis of dyes and phenol solution in the whole experiments was neglectable. All the above results verified that the synergetic effects between Ag@AgCl and ZSH are crucial which lead to effective transfer and separation of photoinduced charge carriers and provide guidance for the construction of high-quality photocatalysts, ultimately emerged as a remarkable photocatalytic activity.

Notably, the recyclability and stability of the as-prepared photocatalysts is one of the most important parts for practical application. The consecutive runs of photocatalytic degradation of RhB and CV solution by Ag@AgCl/ZSH-20 sample under visible light irradiation were also investigated. The as-prepared

Ag@AgCl/ZSH-20 sample had been performed five reaction runs under the same operational condition, for each cycle the catalyst was recycled by centrifugation and washed with de-ionized water, and then dried at 80 °C for further reuse. As displayed in Figure 12, the degradation efficiencies exhibited no obvious reduction. The XRD patterns (Figure S3) of Ag@AgCl/ZSH-20 after five recycling experiment was almost identical when compared the fresh sample with used one (only the intensity of the peak with a slight weaken), manifesting that physicochemical features of the catalyst was durable and integral. Therefore, the Ag@AgCl/ZSH composite exhibited greatly improved capacity in degradation of organic pollutants, promoting future development into the practical application of novel VLD photocatalysts.

4. Possible photocatalytic mechanism

To understand the mechanism of the photocatalytic oxidation process thoroughly, it is essential to detect the main oxidative species formed in the Ag@AgCl/ZSH composite. Thereby, a trapping experiment was developed by adding different types of active species scavengers in the catalyst system. According to the previous researches, three typical chemical reagents, isopropanol (IPA, [43] a quencher of •**OH**), Trietjanolamine (TEOA, [44] a quencher of h^+) and Benzoquinone (BQ, [45] a quencher of $•O^{2-}$), were adopted to interpret the photocatalytic reactions. Prior to irradiation, the corresponding scavengers (10 mM) were added into the RhB aqueous solution along with the photocatalysts. It can be noticed from Fig. 13 that the photodegradation efficiency of RhB and CV decreased significantly by BQ, indicating that $•O^{2-}$ acted as the dominant active species responsible for the degradation of organic pollutants

405 under visible-light irradiation. Meanwhile, the TEOA also resulted in considerable
406 suppression of photocatalytic activity of Ag@AgCl/ZSH-20 and the efficiencies
407 decreased from 99.86% (98.56%) to 53.94% (33.26%) for RhB (CV) degradation,
408 respectively, suggesting that h^+ also played important role in this visible-light
409 photodegradation process. The insignificant fall for the photodegradation efficiency of
410 RhB and CV in the presence of IPA showed that the effect of •OH was weak, thus the
411 effect of •OH could be ignored. The direct photocatalytic oxidation mechanism should
412 be response for the highly enhanced photocatalytic activities, which is in accordance
413 with the previous studies [46].

414 Most importantly, to give a definite insight into the photodegradation mechanism
415 of organic pollutants by Ag@AgCl/ZSH composites, the relative band positions of
416 two semiconductors should be determined, due to its pivot role in the excitation,
417 migration and recombination of the photogenerated electrons and hairs. The band
418 edge positions of conduction band (CB) and valence band (VB) of Ag@AgCl/ZSH
419 composite at the point of zero charge could be theoretically predicted by the following
420 formula: [47]

421 $$E_{CB}=X-E_e+0.5E_g \quad (2)$$

422 $$E_{VB}=E_{CB}+E_g \quad (3)$$

423 where E_{CB} is the conduction band (CB) potentials, E_{VB} is the valence band (VB)
424 potentials. X is the absolute electronegativity of the semiconductor, which is the
425 geometric mean of the electronegativity of the constituent atoms. E_e is the energy of
426 free electrons on the hydrogen scale (≈ 4.5 eV) and E_g is the band gap energy of the

semiconductor. Besides, the conduction band bottom (E_{CB}) and the valence band bottom (E_{VB}) of AgCl are calculated to -0.06 and 3.2 eV, respectively. [48-50] The CB and VB energy levels of ZSH are estimated to be 0.49 and 4.2 eV, respectively.

On the basis of the above-described experimental studies, a possible mechanism for the photocatalytic activity enhancement of Ag@AgCl/ZSH composite was proposed and schematically illustrated in Scheme 1. Learning from the previous researches, the electron-hole recombination is a vital reason for the decrease of the photocatalytic activity. Thus, suppressing the recombination processes of photogenerated electrons and holes is essential to improve the photocatalytic performance. Furthermore, it is well known that Ag@AgCl is an efficient visible-light photocatalyst, even though with the wide band gap, which is attributing to the plasmonic absorption of metallic Ag nanoparticles. [51-52] Thus the excitation occurring over the coupled Ag@AgCl could not originate from the excitation of AgCl. As shown in Scheme 1, under visible light irradiation, however neither ZSH nor AgCl could be stimulated by the visible light on account of the wide band gap of 3.71 eV and 3.26 eV, respectively. Only Ag nanoparticles can absorb the visible light and generate electron-hole pairs thanks to its SPR effect and dipolar characteristic and the forming photogenerated electron-hole pairs could be efficiently separated in the surface of Ag NPs. [33, 34, 43] The plasmon-induced electrons of Ag particles are transported to the CB of AgCl and further flow to the CB of ZSH, owing to the CB potential of AgCl (-0.06 eV) is more negative than that of ZSH (+0.42 eV). Simultaneously, a certain amount of photogenerated h^+ originating from Ag NPs

449 transfers to the surface of AgCl particles and ending up with Cl^- and Ag^0 under visible
450 light irradiation. Moreover, the transferred h^+ could oxidize chlorine (Cl^-) to Cl^0 atoms.
451 [53, 54] As chlorine atoms are reactive radical species, thus they could oxidize the
452 organic pollutants and become reduced to chloride ion again, which could achieve a
453 chlorine recycling for long-term application. At the same time, the partial e^- on the
454 surface of the Ag NPs are trapped by dissolved O_2 to form the reactive specie $\bullet O_2^-$,
455 which could oxidize the organic pollutants. As mentioned above, the major reactions
456 occurring in the photodegradation of organic pollutants were listed as follows:

457 $Ag + h\gamma \rightarrow Ag\ (h^+) + Ag\ (e^-)$ (4)

458 $Ag\ (e^-) + AgCl \rightarrow AgCl\ (e^-) + Ag$ (5)

459 $Ag\ (e^-) + ZSH \rightarrow ZSH\ (e^-) + Ag$ (6)

460 $Ag\ (h^+) + AgCl \rightarrow Ag + Cl^0$ (7)

461 Cl^0 +organic pollutant $\rightarrow CO_2 + H_2O + Cl^-$ (8)

462 $Ag\ (e^-) + O_2 \rightarrow Ag + \bullet O^{2-}$ (9)

463 $\bullet O^{2-}$, h^+, Cl^0 +organic pollutant$\rightarrow CO_2 + H_2O$ (10)

464 According to the previous studies, the photoluminescence (PL) spectrum is an
465 effective approach to evaluate the migration, transfer and recombination properties of
466 the photogenerated electron-hole pairs in the forming semiconductor. In order to
467 confirm the intrinsic separation of the photogenerated charges of the as-prepared
468 samples, the PL emission spectrum of ZSH and Ag@Ag/ZSH-20 were displayed in
469 Figure 14. It could clearly be found out that ZSH showed a high emission peak while
470 the PL emission intensities of Ag@AgCl/ZSH-20 decreased after the introduction of

Ag@AgCl, which suggested the recombination of charge carrier was prevented effectively and lead to improved charge carrier separation in the Ag@AgCl/ZSH-20 composite.

5. Conlusions

In summary, an efficient visible light responsive plasmonic photocatalyst Ag@AgCl/ZSH has been successfully synthesized through anchoring AgCl nanoparticles on the surface and vicinity of ZSH nanoboxes followed by photoreducing partial Ag^{+} ions of AgCl NPs to Ag^{0} species. The as-prepared Ag@AgCl/ZSH displayed excellent improved photocatalytic performace under visible light irradiation, of which Ag@AgCl (8 wt%)/ZSH-20 showed the highest photocatalytic acivity over the photodegradation of RhB and CV dyes and phenol solution at room temperature. The above achieved results indicated that the novel visible-light-driven photocatalyst of Ag@Ag/ZSH not only possessed high photocatalytic activity in degradation of colored dyes but only displayed a potential application in the decomposition of the complex organic and colourless pollutants. The remarkably enhanced photocatalytic performance of the Ag@AgCl/ZSH composite owing to the strong SPR absorption of Ag NPs and efficient electron transfer in the photocatalytic system, leading to lower recombination rates of photo-induced electron-hole pairs. Through trapping experiment, $\bullet O^{2-}$and H^{+} acted as the dominant active species producing in the photocatalytic process. This work could provide new insights into designing of plasma-based photocatalysts with highly efficient photocatalytic properties for promising application in the areas of

493 environmental improvement and energy issues.

494

495 **Acknowledgements**

496 This research was financially supported by the project of National Natural Science
497 Foundation of China (NSFC) (Nos. 51278175, 51378188, 51478170) and Doctoral
498 Fund of Ministry of Education of China (20130161120021)

499

500 **References:**

501 [1] BO. O'Regan, M. Gratzel, A Low-cost, High-efficiency Solar Cell Based on
502 Dye-sensitized Colloidal TiO_2 Films, *Nature*, 1991, **353**, 737-740.

503 [2] X. Chen, S.S. Mao, Titanium Dioxide Nanomaterials: Synthesis, Properties,
504 Modifications, and Applications, *Chem. Rev.*, 2007, **107**, 2891-2959.

505 [3] H. Tong, S. Ouyang, Y. Bi, N. Umezawa, M. Oshikiri, J. Ye, Nano-photocatalytic
506 materials: possibilities and challenges, *Adv. Mater.*, 2012, **24,** 229-251.

507 [4] G. Xi, J. Ye, Q. Ma, N. Su, H. Bai, C. Wang, In situ growth of metal particles on
508 3D urchin-like WO_3 nanostructures, *J. Am. Chem. Soc.*, 2012, **134**, 6508-6511.

509 [5] C.J. Li , S.P. Wang , T. Wang , Y.J. Wei , P. Zhang, J.L. Gong, Monoclinic Porous
510 $BiVO_4$ Networks Decorated by Discrete g-C_3N_4 Nano-Islands with Tunable Coverage
511 for Highly Efficient Photocatalysis, *Small*, 2014, **10**, 2783-2790.

512 [6] T.S. Natarajan, M. Thomas, K. Natarajan, H.C. Bajaj, R.J. Tayade, Study on
513 UV-LED/TiO_2 process for degradation of Rhodamine B dye, *Chem. Eng. J*, 2011, **169**,
514 126-134.

[7] S. Linley, T. Leshuk, F.X. Gu, Synthesis of magnetic rattle-type nanostructures for use in water treatment, *Appl. Mater. Interfaces*, 2013, **5** 2540-2548.

[8] X.B. Chen, S.H. Shen, L.J. Guo, S.l Mao, Semiconductor-based photocatalytic hydrogen generation, *Chem. Rev.*, 2010, **110**, 6503-6570.

[9] A, Kudo, Y. Miseki, Heterogeneous photocatalyst materials for water splitting, *Chem. Soc. Rev.*, 2009, **38**, 253-278.

[10] Z.A. Huang, Q. Sun, K.L. Lv, Z.H. Zhang, M. Li, B. Li, Effect of contact interface between TiO_2 and g-C_3N_4 on the photoreactivity of g-C_3N_4/TiO_2 photocatalyst: (001) vs (101) facets of TiO_2, *Appl. Catal. B: Environ.*, 2015, **164**, 420-427.

[11] Z.F. Jiang, D.L. Jiang, Z.X. Yan, D. Liu, K. Qian, J.M. Xie, A new visible light active multifunctional ternary composite based on TiO_2-In_2O_3 nanocrystals heterojunction decorated porous graphitic carbon nitride for photocatalytic treatment of hazardous pollutant and H_2 evolution, *Appl. Catal. B: Environ.*, 2015, **170-171**, 195-205.

[12] Y.S. Xu, W.D. Zhang, Anion exchange strategy for construction of sesame-biscuit-like $Bi_2O_2CO_3$/Bi_2MoO_6 nanocomposites with enhanced photocatalytic activity, *Appl. Catal. B: Environ.*, 2013, **140-141**, 306-316.

[13] Q.W. Zhu, Y.H. Zhang, F.S. Zhou, F.Z. Lu, Z.F. Ye, F.D. Fan, Preparation and characterization of Cu_2O-ZnO immobilized on diatomite for photocatalytic treatment of red water produced from manufacturing of TNT, *Chem. Eng. J*, 2011, **171**, 61-68.

[14] S. Shenawi-Khalil, V. Uvarov, S. Fronton, I. Popov, Y. Sasson, A novel

heterojunction BiOBr/Bismuth oxyhydrate photocatalyst with highly enhanced visible light photocatalytic properties, *J. Phys. Chem. C*, 2012, **116**, 11004-11012.

[15] Z.H. Li, Z.P. Xie, Y.F. Zhang, L. Wu, X.X. Wang, X.Z. Fu, Wide band gap p-block metal oxyhydroxide InOOH: a new durable photocatalyst for benzene degradation, *J. Phys. Chem. C*, 2007, **111**, 18348-18352.

[16] Y.B. Chen, D.Z. Li, M. He, Y. Hu, H. Ruan, Y.M. Lin, J.H. Hu, Y. Zheng, Y. Shao, High photocatalytic performance of zinc hydroxystannate toward benzene and methyl orange, *Appl. Catal. B: Environ.*, 2012, **113-114**, 134-140.

[17] J.Z. Xu, C.Y. Zhang, H.Q. Qu, C.M. Tian, Zinc hydroxystannate and zinc stannate as flame-retardant agents for flexible poly (vinyl chloride), *J. Appl. Polym. Sci.*, 2005, **98**, 1469-1475.

[18] W.H. Feng, Z.X. Pei, Z.B. Fang, A novel high-photoactivity quaternary ZnSn $(OH)_6$ graphene composite evolved from a 3D multilayer structure via a facile and green proton-mediated self-assembly method. *J. Mater. Chem. A*, 2014, **2(21)**, 7802-7811.

[19] R.M. Liu, Y.W. Jiang, F. Gao, W. Du, Q.Y. Lu, Biopolymer-assisted construction and gas-sensing study of uniform solid and hollow ZSH spheres, *Sensor. Actuat. B-Chem.*, 2013, **178**, 119-124.

[20] Q. He, J.F. Zi, B.J. Huang, L.Y. Yan, W.J. Fa, D.P. Li, Y.G. Zhang,Y.H. Gao, Z. Zheng, Controlled growth and thermal decomposition of well-dispersed and uniform ZSH submicrocubes, *J. Alloy. Compd.*, 2014, **607**, 193-197.

[21] X.L. Fu, X.X. Wang, Z.X. Ding, J.L. Long, W.X. Zhang, Z.H. Li, X.Z. Fu,

559 Hydroxide ZSH: A promising new photocatalyst for benzene degradation, *Appl. Catal.*
560 *B: Environ.*, 2009, **91**, 67-72.
561 [22] H.Q. Li, Y.M. Cui, W.S. Hong, B.L. Xu, Enhanced photocatalytic activities of
562 BiOI/ZSH composites towards the degradation of phenol and photocatalytic H_2
563 production, *Chem. Eng. J*, 2013, **228**, 1110-1120.
564 [23] D. Tsukamoto, Y. Shiraishi, Y. Sugano, S. Ichikawa, S.Tanaka, T. Hirai, Gold
565 nanoparticles nocated at the Interface of anatase/rutile TiO_2 Particles as Active
566 plasmonic photocatalysts for Aerobic Oxidation. *J. Am. Chem. Soc.*, 2012, **134**,
567 6309-6315.
568 [24] Z.J. Zhou, M.C. Long, W.M. Cai, J. Cai, Synthesis and photocatalytic
569 performance of the efficient visible light photocatalyst Ag-AgCl/$BiVO_4$, *J. Mol. Catal.*
570 *A: Chem.*, 2012, **353-354**, 22-28.
571 [25] X.X. Hu, C. Hu, T.W. Peng, X.F. Zhou, J.H. Qu, Plasmon-induced inactivation of
572 enteric pathogenic microorganisms with Ag-AgI/Al_2O_3 under visible-light irradiation,
573 *Environ. Sci. Technol.*, 2010, **44**, 7058-7062.
574 [26] J. Ke, C.G. Niu, J. Zhang, G.M. Zeng, Significantly enhanced visible light
575 photocatalytic activity and surface plasmon resonance mechanism of
576 Ag/AgCl/$ZnWO_4$ composite, *J. Mol. Catal. A: Chem.*, 2014, **395**, 276-282
577 [27] B. Li, H. Wang, B.W. Zhang, P.F. Hu, C. Chen, L. Guo, Facile synthesis of one
578 dimensional AgBr@Ag nanostructures and their visible light photocatalytic properties,
579 *Appl. Mater. Interfaces*, 2013, **5**, 12283-12287.
580 [28] C.H. An, J.Z. Wang, W. Jiang, M.Y. Zhang, X.J. Ming, S.T. Wang, Q.H. Zhang,

581 Strongly visible-light responsive plasmonic shaped AgX: Ag (X= Cl, Br)
582 nanoparticles for reduction of CO_2 to methanol, *Nanoscale*, 2012, **4**, 5646-5650.
583 [29] P. Wang, B. Huang, X. Zhang, X. Qin, H. Jin, Y. Dai, Z. Wang, J. Wei, J. Zhan, S.
584 Wang, J. Wang, M.H. Whangbo, Highly Efficient Visible□Light Plasmonic
585 Photocatalyst Ag@ AgBr, *Chem. Eur. J.*, 2009, **15**, 1821-1824.
586 [30] P. Wang, B. Huang, Q. Zhang, X. Zhang, X. Qin, Y. Dai, J. Zhan, J. Yu, H. Liu, Z.
587 Lou, Highly efficient visible light plasmonic photocatalyst Ag@ Ag (Br, I), *Chem. Eur.*
588 *J.*, 2010, **16**, 10042-10047.
589 [31] X.X. Li, S.M. Fang, L. Ge, C.C. Han, P. Qiu, W.L. Liu, Synthesis of flower-like
590 Ag/AgCl-Bi_2MoO_6 plasmonic photocatalysts with enhanced visible-light
591 photocatalytic performance, *Appl. Catal. B: Environ.*, 2015, **176**, 62-69
592 [32] K. Fuku, R. Hayashi, S. Takakura, T. Kamegawa, K. Mori, H. Yamashita, The
593 Synthesis of Size and Color Controlled Silver Nanoparticles by Using Microwave
594 Heating and their Enhanced Catalytic Activity by Localized Surface Plasmon
595 Resonance, Angew. *Chem. Int. Ed.*, 2013, **52**, 7446-7450.
596 [33] T. Morimoto, K. Suzuki, M. Torikoshi, T. Kawahara, H. Tada, Ag (core) - AgCl
597 (shell) standard microelectrode - loaded TiO_2, *Chem. Commun.*, 2007, **41**, 4291-4293.
598 [34] B.W. Ma, J.F. Guo, W.L. Dai, K.N. Fan, Ag-AgCl/WO_3 hollow sphere with
599 flower-like structure and superior visible photocatalytic activity, *Appl. Catal. B:*
600 *Environ.*, 2012, **123-124**, 193-199.
601 [35] S.W. Zhang, J.X. Li, X.K. Wang, Y.S. Huang, M.Y. Zeng, J.Z. Xu, In Situ Ion
602 Exchange Synthesis of Strongly Coupled Ag@AgCl/g-C_3N_4 Porous Nanosheets as

603 Plasmonic Photocatalyst for Highly Efficient Visible-Light Photocatalysis, *Appl.*
604 *Mater. Interface*, 2014, **6**, 22116-22125.
605 [36] Y.H. Liang, S.L. Lin, L. Liu, J.S. Hu, W.Q. Cui, Oil-in-water self-assembled
606 Ag@AgCl QDs sensitized Bi_2WO_6: Enhanced photocatalytic degradation under
607 visible light irradiation, *Appl. Catal. B: Environ.*, 2015, **164,** 192-203.
608 [37] C. Hu, J. Guo, J.H. Qu, X.X. Hu, Photocatalytic degradation of pathogenic
609 bacteria with AgI/TiO_2 under visible light irradiation, *Langmuir*, 2007, **9(23)**,
610 4982-4987.
611 [38] K. Maeda, Y. Shimodaira, B. Lee, K. Teramura, D. Lu, H. Kobayashi, K. Domen,
612 Studies on $TiN_xO_yF_z$ as a visible-light-responsive photocatalyst, *J. Phys. Chem. C*,
613 2007, **111(49)**, 18264-18270.
614 [39] Z.Q. He, Y.Q. Shi, C. Gao, L. Wen, J.M. Chen, S. Song, BiOCl/$BiVO_4$ p-n
615 heterojunction with enhanced photocatalytic activity under visible-light irradiation, *J.*
616 *Phys. Chem. C*, 2014, **118**, 389-398.
617 [40] J.G. Hou, Z. Wang, C. Yang, W.L. Zhou, S.Q. Jiao, H.M. Zhu, Hierarchically
618 Plasmonic Z-Scheme Photocatalyst of Ag/AgCl Nanocrystals Decorated Mesoporous
619 Single-Crystalline Metastable $Bi_{20}TiO_{32}$ Nanosheets, *J. Phys. Chem. C*, 2013, **117**,
620 5132-5141.
621 [41] L.Q. Ye. J.Y. Liu; C.Q. Gong, L.H. Tian, T.Y. Peng, L. Zan, Two different Roles
622 of Metallic Ag on Ag/AgX/BiOX (X = Cl, Br) Visible Light Photocatalysts: Surface
623 Plasmon Resonance and Z-Scheme Bridge, *ACS Catal.*, 2012, **2** 1677-1683.

624 [42] C.Z. Luo, D.L. Li, W.H. Wu, C.Z. Yu, W.P. Li, C.X. Pan, Preparation of 3D
625 reticulated ZnO/CNF/NiO heteroarchitecture for high-performance photocatalysis,
626 *Appl. Catal. B: Environ.*, 2015, **166-167**, 217-223.
627 [43] X. Zhang, T. Guo, X.. Wang, Y. Wang, C. Fan, H. Zhang, Facile
628 composition-controlled preparation and photocatalytic application of
629 $BiOCl/Bi_2O_2CO_3$ nanosheets, *Appl. Catal. B: Environ.*, 2014, **150-151**, 486-495.
630 [44] J.C. Sun, Y.B. Zhang, J. Cheng, H. Fan, J.Y. Zhu, X. Wang, S.Y. Ai, Synthesis of
631 Ag/AgCl/Zn-Cr LDHs composite with enhanced visible-light photocatalytic
632 performance, *J. Mol. Catal. A Chem.*, 2014, **382**, 146-153.
633 [45] L.H. Yu, W. Chen, D.Z. Li, J.B. Wang, Y. Shao, M. He, P. Wang, X.Z. Zheng,
634 Inhibition of photocorrosion and photoactivity enhancement for ZnO via specific
635 hollow ZnO core/ZnS shell structure, *Appl. Catal. B: Environ.*, 2015, **164**, 453-461.
636 [46] J.X. Shu, Z.H. Wang, G.Q. Xia, Y.Y. Zheng, L.H. Yang, W. Zhang, One-pot
637 synthesis of AgCl@Ag hybrid photocatalyst with high photocatalytic activity and
638 photostability under visible light and sunlight irradiation, *Chem. Eng. J.*, 2014, **252**,
639 374-381
640 [47] X. Zhang, Z.H. Ai, F.L. Jia, L.L. Zhang, Generalized One-Pot Synthesis,
641 Characterization, and Photocatalytic Activity of Hierarchical BiOX (X = Cl, Br, I)
642 Nanoplate Microspheres. *J. Phys. Chem. C*, 2008, **112(3)**, 747-753.
643 [48] J.G. Hou, C. Yang, Z. Wang, Q.H. Ji, Y.T. Li, G.C. Huang, S.Q. Jiao, H.M. Zhu,
644 Three-dimensional Z-scheme AgCl/Ag/-TaON heterostructural hollow spheres for
645 enhanced visible-light photocatalytic performance, *Appl. Catal. B: Environ.*, 2013,

142-143, 579-589.

[49] S. Linic, P. Christopher, D.B. Ingram, Plasmonic-metal nanostructures for efficient conversion of solar to chemical energy, *Nat. Mater.*, 2011, **10**, 911-921.

[50] R. Liu, P. Wang, X.F. Wang, H.G. Yu, J.G. Yu, UV- and Visible-Light Photocatalytic Activity of Simultaneously Deposited and Doped Ag/Ag(I)-TiO_2 Photocatalyst, *J. Phys. Chem. C*, 2012, **116**, 17721-17728.

[51] G.Q. Luo, X.J. Jiang, M.J. Li, Q. Shen, L.M. Zhang, H.G. Yu, Facile Fabrication and Enhanced Photocatalytic Performance of Ag/AgCl/rGO Heterostructure Photocatalyst, *Appl. Mater. Interfaces*, 2013, **5**, 2161-2168.

[52] P. Wang, B.B. Huang, Y. Dai, Plasmonic photocatalysts : harvesting visible light with noble metal nanoparticles, *Phys. Chem. Chem. Phys.*, 2012, **14**, 9813-9825.

[53] P. Wang, B.B. Huang, X.Y. Qin, X.Y. Zhang, Y. Dai, J.Y. Wei, M. Whang bo, Ag@AgCl: A Highly Efficient and Stable Photocatalyst Active under Visible Light, Angew. *Chem. Int. Ed.*, 2008, **47**, 7931-7933.

[54] J.G. Yu, G.P. Dai, B.B. Huang, Fabrication and Characterization of Visible-Light-Driven Plasmonic Photocatalyst Ag/AgCl/TiO_2 Nanotube Arrays, *J. Phys. Chem. C*, 2009, **113**, 16394-16401.

Figure captions:

Figure 1 XRD patterns of pure ZSH and Ag@AgCl/ZSH composites with different photo-reduction time.

Figure 2 SEM images of the samples: (a, b) pure ZSH and (c, d) Ag@AgCl/ZSH-20 composite.

Figure 3 TEM images with different magnification (a-c); EDX (d).

Figure 4 XPS spectra of Ag@AgCl/ZSH-20 composite.

Figure 5 FTIR spectra of the samples: (a) pure ZSH and (b) Ag@AgCl/ZSH-20 composite.

Figure 6 UV-vis diffuse reflectance spectrum of the samples: (a) pure ZSH and (b) Ag@AgCl/ZSH-20 composite.

Figure 7 Photodegradation of RhB by ZSH, N-doped TiO_2 and various weight ratios of Ag@AgCl/ZSH photocatalysts.

Figure 8 Visible-light photocatalytic degradation of (a) RhB and (b) CV solution for various samples: ZSH, N-doped TiO_2 and Ag@AgCl/ZSH photocatalysts.

Figure 9 The temporal absorption spectrum changes of (a) RhB and (b) CV aqueous solution in the presence of Ag@AgCl/ZSH-20 composite under visible light irradiation.

Figure 10 The photodegradation of phenol with ZSH, N-doped TiO_2 and Ag@AgCl/ZSH-20 composite.

Figure 11 The first-order-kinetics of RhB (a) and CV (b) degradation in the presence of ZSH, N-doped TiO_2 and Ag@AgCl/ZSH photocatalysts.

690 **Figure 12** The cycling degradation efficiency for RhB (a) and CV (b) of
691 Ag@AgCl/ZSH-20 sample under visible light irradiation.
692 **Figure 13** The effects of different scavengers on the degradation of RhB over
693 Ag@AgCl/ZSH-20 under visible light irradiation.
694 **Figure 14** Photoluminescence spectra (PL) of the ZSH and Ag@AgCl/ZSH-20
695 composite.
696 **Scheme 1** Schematic diagram of the photocatalytic mechanism of ZSH loaded with
697 Ag@AgCl.
698
699 **Supplementary Information:**
700 **Figure S1** Comparison of the photocatalytic activities in degradation of RhB by ZSH,
701 Ag@AgCl, Ag-ZSH and Ag@AgCl(8 wt%)/ZSH.
702 **Figure S2** The degradation rate constants of RhB (a) and CV (b) solution with
703 different samples.
704 **Figure S3** The XRD patterns of the used and fresh Ag@AgCl/ZSH-20 in the
705 photodegrdation of RhB solution under visible light irradiation for five consecutive
706 cycles.
707
708
709
710
711

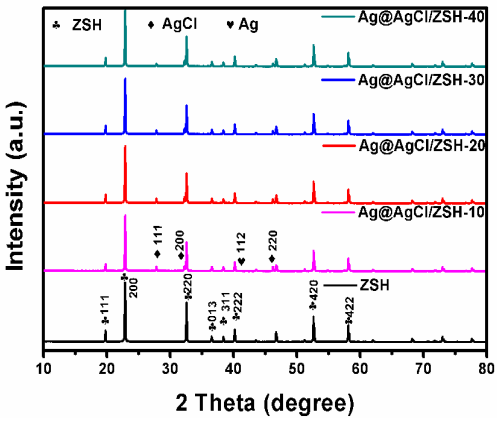

Figure 1 XRD patterns of pure ZSH and Ag@AgCl/ZSH composites with different photo-reduction time.

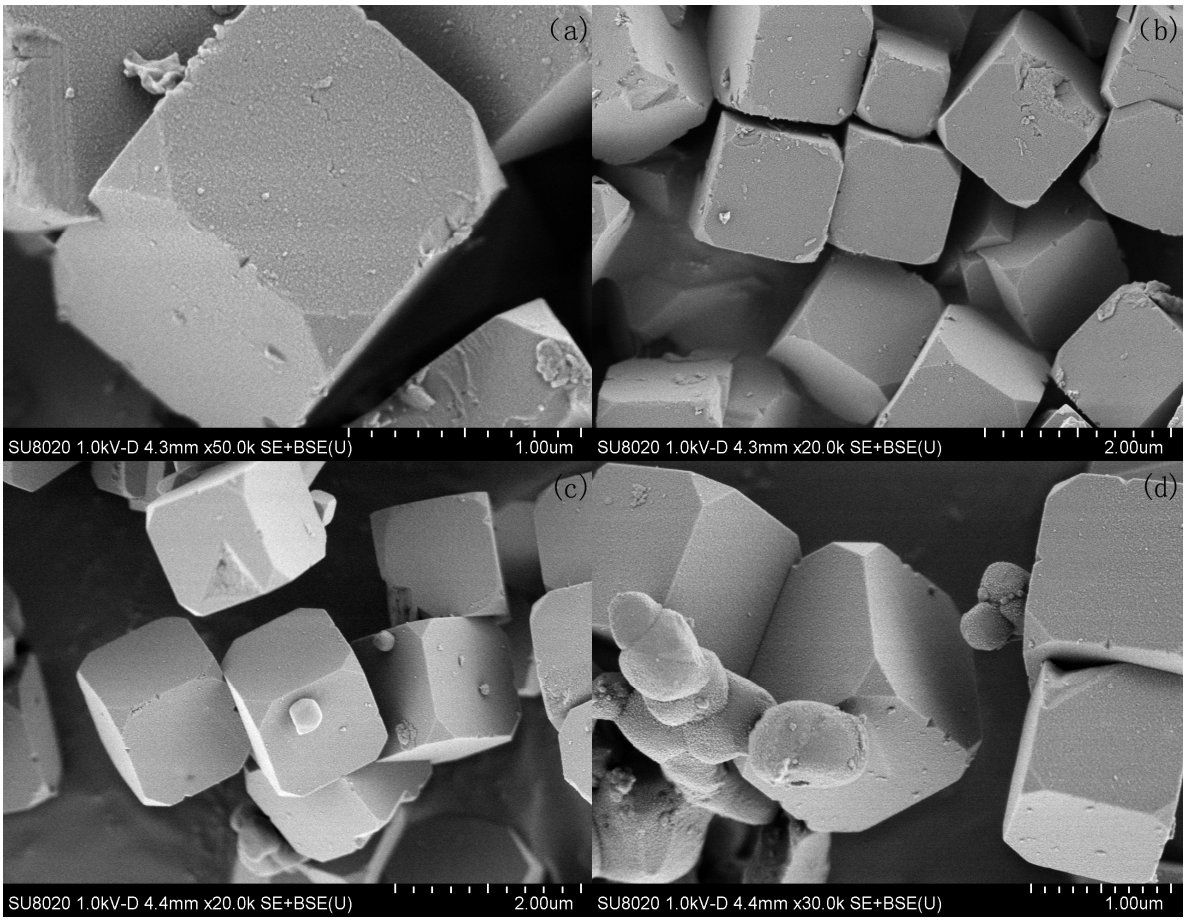

Figure 2 SEM images of the samples: (a, b) pure ZSH and (c, d) Ag@AgCl/ZSH-20 composite.

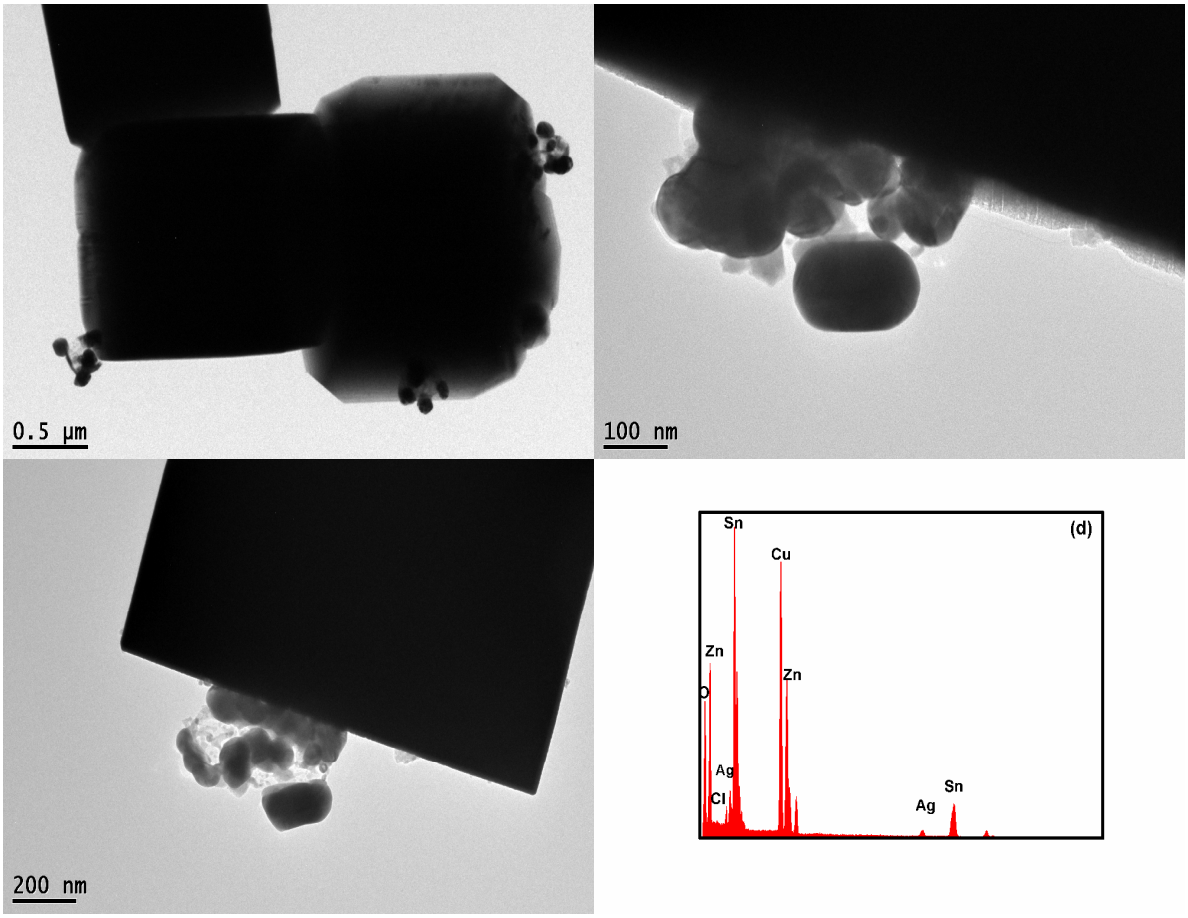

Figure 3 TEM images with different magnification (a-c); EDS (d).

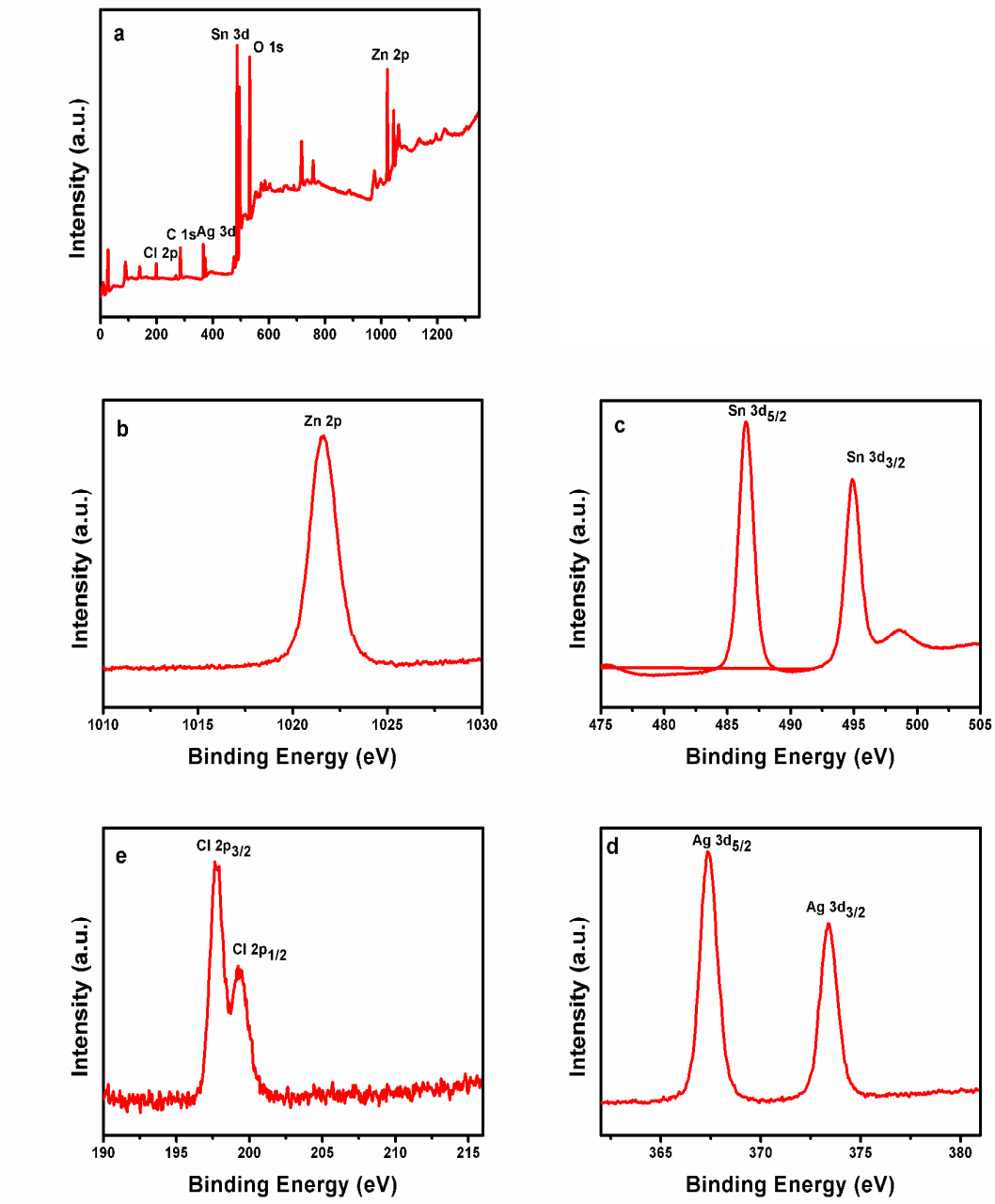

Figure 4 XPS spectra of Ag@AgCl/ZSH-20 composite.

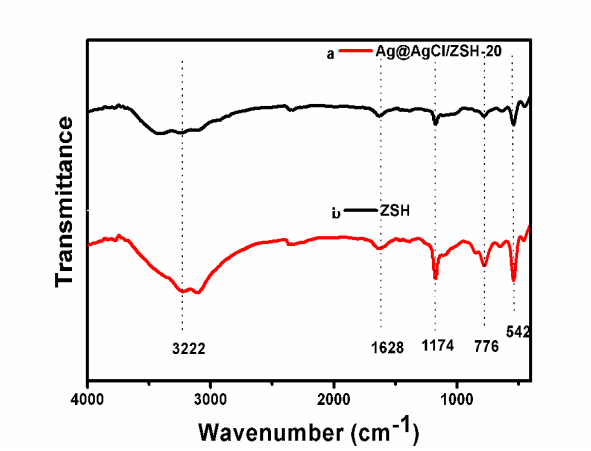

Figure 5 FTIR spectra of the samples: (a) pure ZSH and (b) Ag@AgCl/ZSH-20 composite.

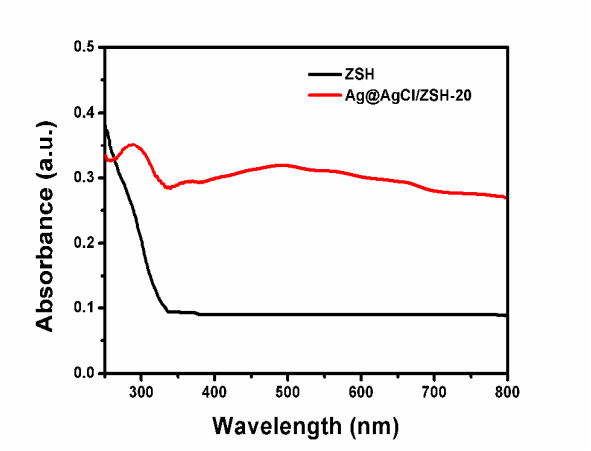

Figure 6 UV-vis diffuse reflectance spectrum of the samples: (a) pure ZSH and (b) Ag@AgCl/ZSH-20 composite.

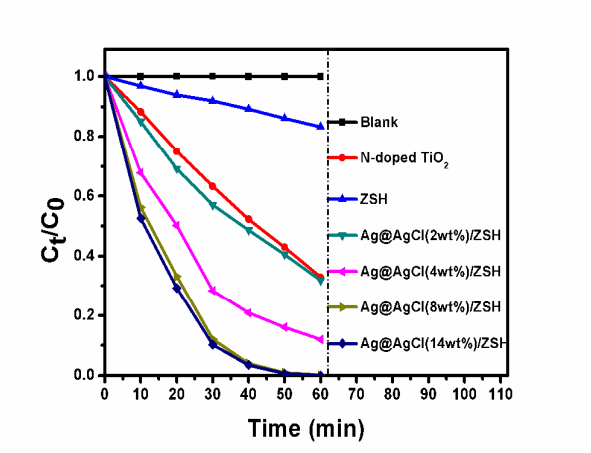

Figure 7 Photodegradation of RhB by ZSH, N-doped TiO_2 and various weight ratios of Ag@AgCl/ZSH photocatalysts.

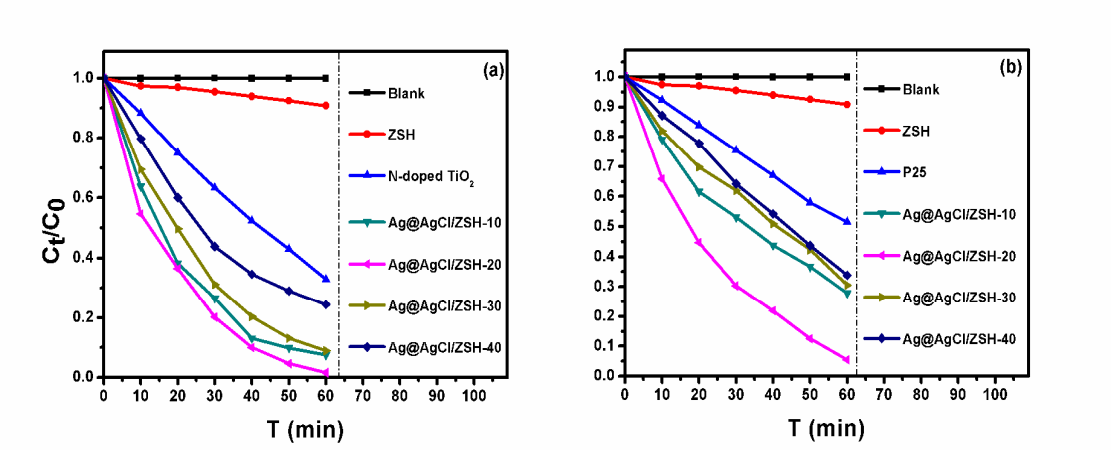

Figure 8 Visible-light photocatalytic degradation of (a) RhB and (b) CV solution for various samples: ZSH, N-doped TiO_2 and Ag@AgCl/ZSH photocatalysts.

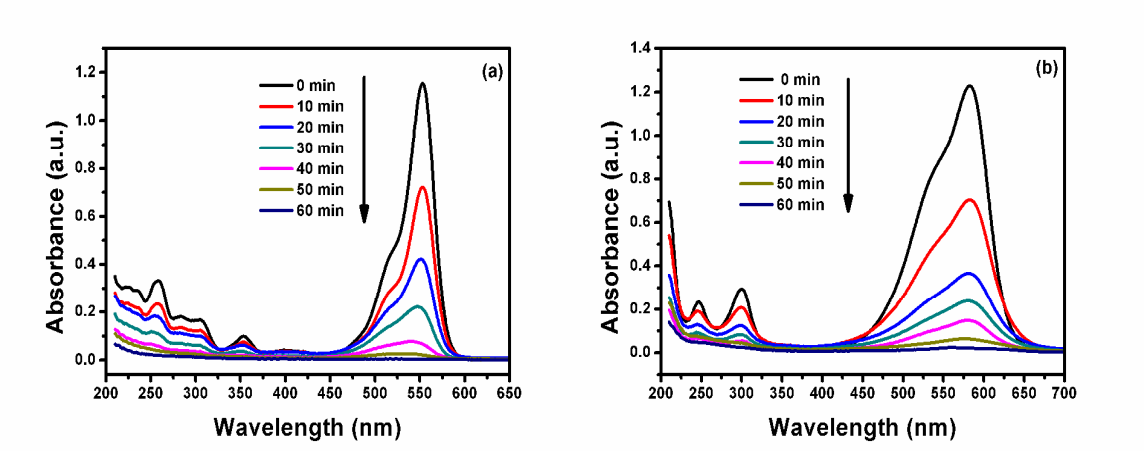

Figure 9 The temporal absorption spectrum changes of (a) RhB and (b) CV aqueous solution in the presence of Ag@AgCl/ZSH-20 composite under visible light irradiation.

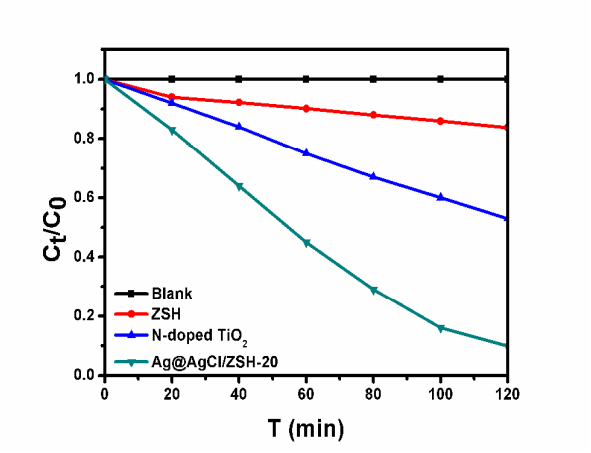

Figure 10 The photodegradation of phenol with ZSH, N-doped TiO_2 and Ag@AgCl/ZSH-20 composite.

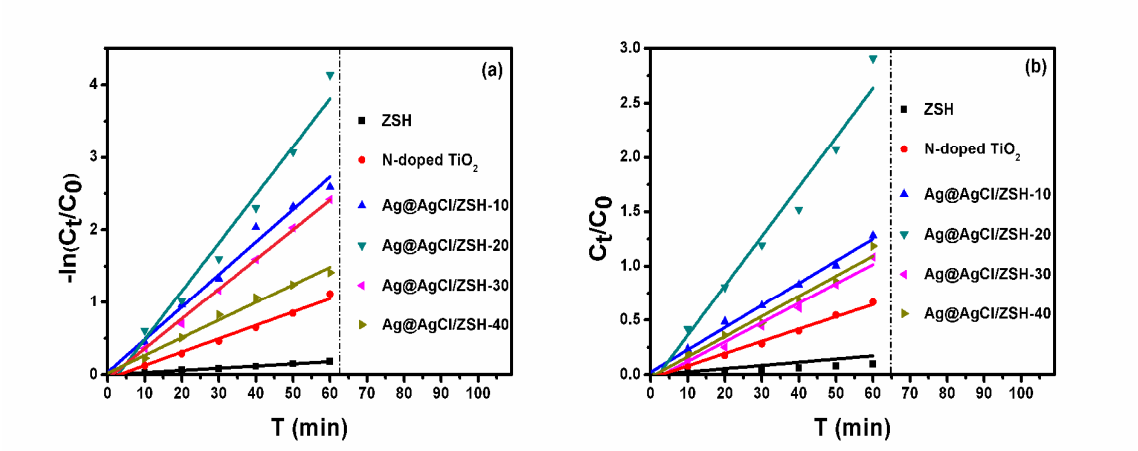

Figure 11 The first-order-kinetics of RhB (a) and CV (b) degradation in the presence of ZSH, N-doped TiO_2 and Ag@AgCl/ZSH photocatalysts.

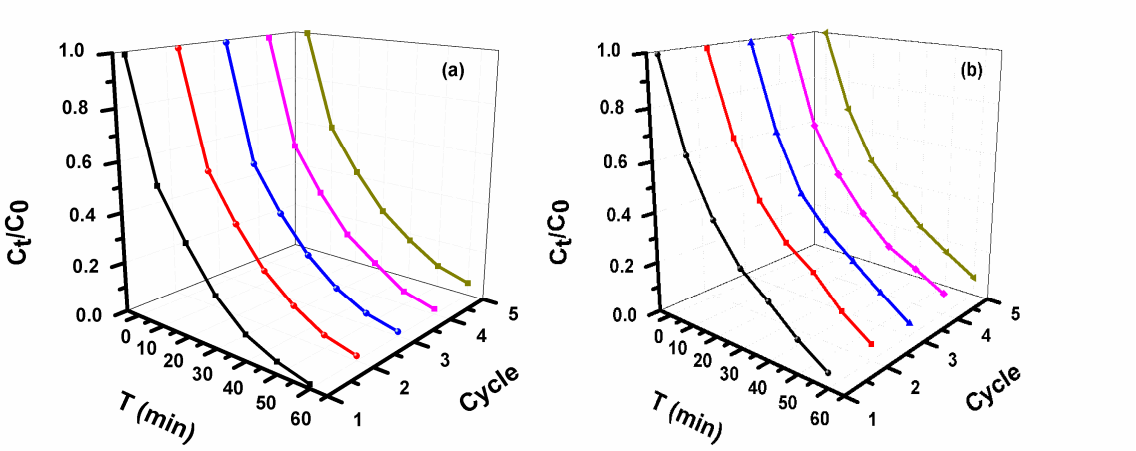

Figure 12 The cycling degradation efficiency for RhB (a) and CV (b) of Ag@AgCl/ZSH-20 sample under visible light irradiation.

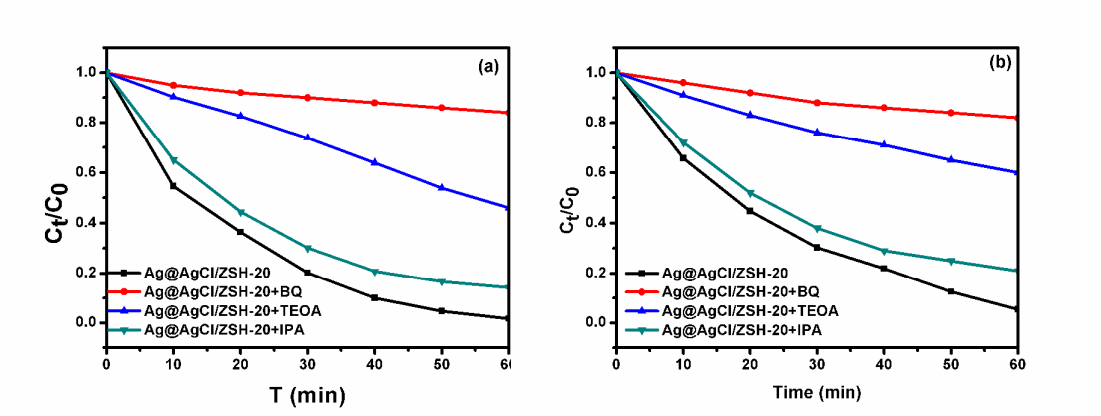

Figure 13 The effects of different scavengers on the degradation of RhB (a) and CV (b) over Ag@AgCl/ZSH-20 under visible light irradiation.

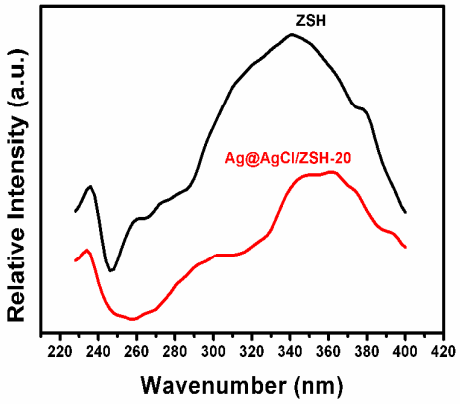

Figure 14 Photoluminescence spectra (PL) of the ZSH and Ag@AgCl/ZSH-20 composite.

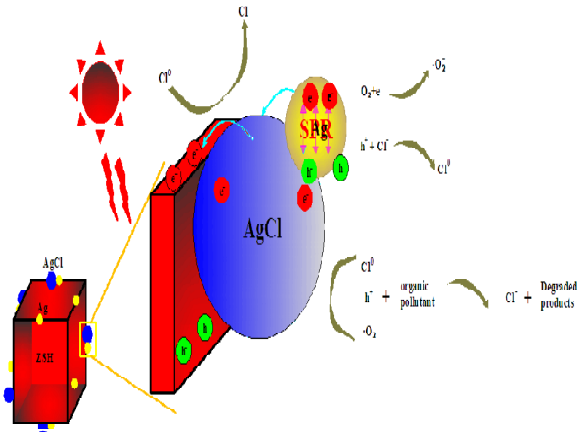

Scheme 1 Schematic diagram of the photocatalytic mechanism of ZSH loaded with Ag@AgCl.

Plasmonic photocatalyst Ag@AgCl/ZnSn(OH)$_6$: Synthesis, characterization and enhanced visible-light photocatalytic activities in the decomposition of dyes and phenol

Fei Chen[a,b], Qi Yang[a,b,*], Chenggang Niu[a,b], Xiaoming Li[a,b], Chang Zhang[a,b], Guangming Zeng[a,b]

[a] College of Environmental Science and Engineering, Hunan University, Changsha 410082, P.R. China

[b] Key Laboratory of Environmental Biology and Pollution Control (Hunan University), Ministry of Education, Changsha 410082, P.R. China

Author information

First author: E-mail: feichen@hnu.edu.cn (Fei Chen)

*Corresponding author:E-mail: Yangqi@hnu.edu.cn

Graphical Abstract

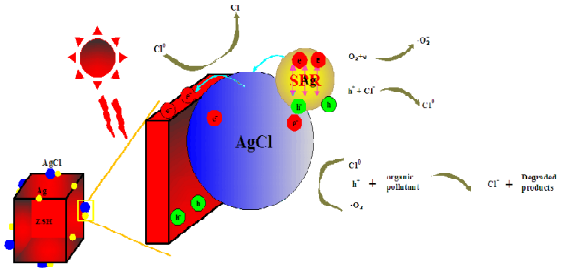

Highlights

1. Efficient VLD photocatalyst Ag@AgCl/ZSH was fabricated by ultrasonic assistant precipitation-photoreduction method

2. Photocatalytic activities were investigated in details;

3. A possible mechanism was discussed thoroughly.